PHYSICAL REVIEW E

STATISTICAL PHYSICS, PLASMAS, FLUIDS, AND RELATED INTERDISCIPLINARY TOPICS

THIRD SERIES, VOLUME 52, NUMBER 4 PART B OCTOBER 1995

ARTICLES

Effects of grafting geometry and solvent quality on the structure of bimodal polymer brushes

Hao Chen and Amitabha Chakrabarti

Department of Physics, Kansas State University, Manhattan, Kansas 66506

(Received 17 February 1995)

We carry out extensive off-lattice computer simulations of bimodal polymer brushes and discuss the effects of different grafting geometry and solvent quality on the structure of such mixed polymer brushes. For a flat grafting surface and good solvents, the short and long chains segregate vertically and the long chains stretch more in the coexisting region. The situation is different for polymers grafted onto a flat surface and in contact with poor solvents where vertical segregation between the long and the short chains is found to be much weaker. Also, as the function of short chains increases in the layer, both the short and the long chains stretch less. This is different from the good solvent case where the stretching of the short chains increases as the short chain fraction increases. For a spherical grafting surface and in good solvents, the stretching of the two type of chains is similar in the inner layer. In a poor solvent, the situation is similar to a flat grafting surface with poor solvents and both types of chains are equally stretched over the entire region of the layer.

PACS number(s): 36.20.−r, 82.70.−y, 87.15.−v, 81.60.Jw

I. INTRODUCTION

A dispersed system, in which colloidal particles are maintained in suspension, is desired in a wide range of areas such as paints, glues, food emulsions, and pharmaceuticals [1]. This stabilization can be achieved by end grafting suitable polymer chains on the surface of the colloidal particles. In such a situation, the repulsion between the resulting polymer layers or "brushes" maintains the colloidal particles in suspension. A proper understanding of the stabilization process thus requires a thorough knowledge of the structure of the polymer brush in various solvent conditions and in the presence of various surface interactions. For this reason, the detailed structure of polymer brushes, as well as the interactions between them, has been the subject of many recent experiments [2–5], theoretical studies [6,7], and extensive computer simulations [8].

While most of the pertinent work mainly has dealt with the monodisperse brush, some theoretical work has also been carried out to understand the effects of polydispersity on the structure of polymer brushes. In experimental situations polydispersity is an often unavoidable feature, which greatly affects the brush structure. This fact is an important motivation for theoretical studies of a polydisperse brush. One finds that polydispersity can actually be used to one's advantage in tailoring specific brush structures. In good solvent conditions and for flat grafting surfaces, a vertical segregation takes place between chains of different molecular weights. Moreover, in the coexisting region of long and short chains, a difference between the local degree of stretching has been observed. Thus the outer region of the brush may be used for various desired functions, such as a specific interaction with another surface.

The structure of the polydisperse brush has been studied theoretically by Milner, Witten, and Cates [9] and by Birstein, Liatskaya, and Zhulina [10]. Chakrabarti and Toral [11] carried out Monte Carlo simulations in a lattice model for both polydisperse and bidisperse polymer brushes. A bimodal molecular weight (chain length) distribution has often been used in simulations as a model system for polydispersity. Subsequently, Lai and Zhulina [12] have studied the bidisperse brush by simulations of a bond-fluctuation model and Dan and Tirrel [13] have studied the bidisperse system by using a numerical self-consistent model. Most of these previous studies considered a good solvent and a flat grafting geometry. A more recent work, however, has addressed the effect of solvent quality on a mixed brush in a *selective solvent* [14].

In this paper, we extend previous work on polydisperse brushes by carrying out detailed simulations on a freely joined hard-sphere model (or "pearl-necklace" model) of polymer chains for various grafting geometries and for various *nonselective* solvents. Previously, this model has been used by us to study the structure of the monodisperse brush grafted onto a spherical surface [15] and the interactions between polymer brushes grafted onto two parallel surfaces [16]. In both cases, the agreement between the simulations and the theoretical results was very good. This fact, together with the computational simplicity, makes the pearl-necklace model a natural choice among the off-lattice models for the study of brushes. In the present work, we consider a brush with a bimodal chain length distribution. Our results for flat

grafting surfaces with good solvents agree quite well with earlier analytical and numerical calculations. Results for spherical grafting surfaces and for flat surfaces with poor solvents are presented and discussed in detail. The rest of the paper is organized as follows. The model and the simulation method are described in Sec. II. Section III presents the numerical results and their comparison with theoretical predictions whenever possible and Sec. IV outlines the main conclusions.

II. MODEL AND NUMERICAL PROCEDURE

We consider a bimodal distribution of chain lengths for polymer molecules grafted onto either a flat surface or a spherical surface under variable solvent conditions. The polymer chains are modeled by the so-called pearl-necklace model. In this model, the long chains and the short chains are considered to be made of N_L and N_S monomers, respectively, linked by rigid rods. Each monomer is modeled as a hard sphere of diameter unity. The distance between successive monomer centers is set to be 1.1 times the diameter. The first monomer ("head") of each chain is permanently anchored onto the grafting surface and consecutive monomers are added by executing a self-avoiding random walk starting from the first monomer. Besides the self- and mutually avoiding interactions (the monomer spheres cannot penetrate each other or the grafting surface), an attractive interaction between monomers is introduced. The total interaction potential between monomers in units of kT can be written as

$$V(r)=\begin{cases}\infty, & r\le 2a\\ -V_0, & 2a<r\le 4a\\ 0, & r>4a\ ,\end{cases} \tag{1}$$

where a is the radius of a hard-sphere monomer and r is the distance between a pair of monomers. We choose several different values for V_0 so that the excluded volume parameter [17]

$$\omega=4\pi\int_0^\infty (1-e^{-V(r)})r^2dr \tag{2}$$

takes both positive and negative values. A positive value of ω corresponds to a good solvent and a negative value corresponds to a solvent poorer than the Θ solvent, which is characterized by $\omega=0$ [18].

For both flat and spherical surfaces, we choose a bimodal chain length distribution with $N_L=2N_S=100$. We consider several values for the short chain fraction f given by $f=0$, 0.25, 0.5, 0.75, and 1. In order to sample the configurations of the system in equilibrium, we simulate the monomer movements by "kink jumps" appropriate for this off-lattice model. The energetics of the system is handled by the standard Metropolis algorithm. Typically, we discard 10^5 Monte Carlo steps (MCS) per monomer for equilibrium and average the quantities over 5×10^4 MCS. Proper equilibrium attained by the system is tested by comparing measured quantities (such as monomer density profiles) obtained when the system evolved from different initial configurations.

In the flat surface case, we consider a total number of N_p chains end grafted onto the $z=0$ surface of a cubic box of size $L_x\times L_y\times L_z$. The centers of the grafted monomers are actually located at $z=1/2$. L_z is chosen to be large enough so that no chain can reach the $z=L_z$ surface. We choose $L_x=L_y=40$ and apply periodic boundary condition in the x and y directions. The total grafting density σ is defined as

$$\sigma=\frac{N_p}{L_xL_y}\ . \tag{3}$$

We considered $N_p=128$ and thus the total grafting density $\sigma=0.08$ for all cases with a flat grafting surface. Among other quantities, we have computed the monomer density defined as

$$\phi_A(z)=\frac{(\text{number of } A\text{-type monomers between } z \text{ and } z+1)}{L_xL_y} \tag{4}$$

and the chain-end density $\epsilon(z)$ given by

$$\epsilon_A(z)=\frac{(\text{number of } A\text{-type end monomers between } z \text{ and } z+1)}{L_xL_y}\ , \tag{5}$$

where A could correspond to a contribution from only short chains $[\phi_S(z),\epsilon_S(z)]$, only long chains $[\phi_L(z),\epsilon_L(z)]$, or all types of chains $[\phi(z),\epsilon(z)]$. The cosine of the angle between the chain segments and the $+z$ direction is calculated as a measure of the degree of stretching of the polymer chains. The cosine of the angle between the ith segment and $+z$ direction is defined as

$$\langle\cos\theta_i\rangle=\left\langle\frac{z_{i+1}-z_i}{r_{i+1}-r_i}\right\rangle\ , \tag{6}$$

where i varies from 1 to N_L-1 for the long chains and from 1 to N_S-1 for the short chains. z_{i+1},z_i are the coordinates of the $(i+1)$th and ith monomers in z direction, $r_{i+1}-r_i=1.1$ is the distance between successive monomers, and the angular brackets indicate both a chain average and an equilibrium average.

For the spherical surface case, we consider the radius R of the grafting sphere to be five times the monomer diameter and the total chain number $N_p=100$. In this case the grafting density σ is defined as

$$\sigma=\frac{N_p}{4\pi R^2}\ , \tag{7}$$

which is 0.32 in our simulations. The monomer density in this case is calculated from

$$\phi_A(r)=\frac{[\text{number of } A\text{-type monomers with distance to origin between } (r+R) \text{ and } (r+R+1)]}{4\pi(r+R+1/2)^2} \tag{8}$$

and the end-chain density is given by

$$\epsilon_A(r)=\frac{[\text{number of } A\text{-type end monomers with distance to origin between } (r+R) \text{ and } (r+R+1)]}{4\pi(r+R+1/2)^2} . \tag{9}$$

Here, again, A could correspond to the contribution from only short chains $[\phi_S(r),\epsilon_S(r)]$, only long chains $[\phi_L(r),\epsilon_L(r)]$, or all types of chains $[\phi(r),\epsilon(r)]$. The stretching of the ith segment $\cos\theta_i$ is defined as

$$\langle\cos\theta_i\rangle=\left\langle\frac{p_{i+1}-p_i}{1.1}\right\rangle , \tag{10}$$

where p_{i+1} and p_i are, respectively, the projections of the coordinates of the $(i+1)$th and ith monomers to the line joining the center of the grafting sphere to the ith monomer.

III. RESULTS

A. Chains in a good solvent

Under good solvent condition, there is no attractive interaction between monomers [$V_0=0$ in Eq. (1)] and they are subjected only to the excluded volume interaction. In this case, the chains stretch normal to the grafting surface and form a (bimodal) polymer brush. We have computed the monomer density, the chain-end density, and the stretching of the individual chains of the bimodal brush for various short chain fractions. In the following we present these results for both flat and spherical grafting surfaces.

1. Flat grafting surface

Monomer and chain-end density profiles are shown in Figs. 1(a) and 1(b) and the stretching of the chains are presented in Fig. 2. In agreement with previous numerical and theoretical results [9–13], we can clearly see the two main features of the bimodal brush: vertical segregation and the difference of the local degree of stretching between the long and short chains. The monomer density profile for the short chains resembles a parabolic form similar to the monodisperse case [19] [Fig. 1(a)]. The long chains are more stretched in the coexisting region and thus the corresponding density profiles have "plateau" regions throughout the inner layer. Close to the grafting surface, the total density of the bimodal brush coincides with that of a monodisperse distribution of chains with length N_S and grafting density $\sigma=0.08$. At a certain distance z_1, these two profiles deviate from each other. This particular distance z_1 increases as the short chain fraction f increases. Numerical values for z_1 are in good agreement with the result of the self-consistent field (SCF) theory [9,10]

$$z_1=\left[\frac{12\omega\sigma}{\pi^2}\right]N_S[1-(1-f)^{2/3}]^{1/2} , \tag{11}$$

where the numerical value for the excluded volume parameter ω is taken from previous simulations ($\omega=1.85$) [16].

The segregation between the long chains and the short chains is also clearly displayed in the chain-end density profiles [Fig. 1(b)]. The total end density profile shows two peaks. The short chain ends are mostly found in the inner region while the longer chains ends are predominantly found in the outer region. There is a crossover region where the ends of both types of chains interpenetrate. With the increase of the short chain fraction f, the end density profile for the short chains shifts away from the grafting surface while that for the long chains shifts toward the surface.

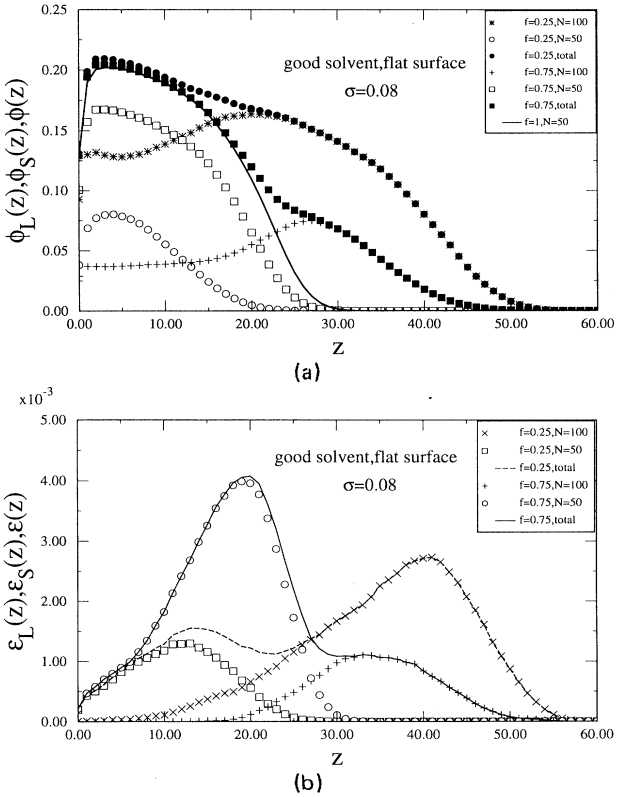

FIG. 1. (a) Density profiles for a bimodal brush grafted onto a flat surface and in contact with a good solvent for different short chain fractions f. The total density and the contribution coming from each type of chains are shown separately. (b) Chain-end density profiles for a bimodal brush grafted onto a flat surface and in contact with a good solvent for different short chain fractions f. The total chain-end density and the contribution coming from each type of chains are shown separately.

Results for the stretching parameter $\cos\theta_i$, for the bimodal brush are shown in Fig. 2 as a function of the monomer number i. It is clear that, regardless of the short chain fraction f in the bimodal brush, the long chains are always more stretched than the short ones. This is in agreement with the SCF theory and previous numerical results. As the short chain fraction f increases, the stretching parameter for the short chains increases and so does this quantity for the long chain segments in the coexisting region. However, in the outer region where only long chain exists, $\cos\theta_i$ for the long chains decreases when f increases, due to the "dilution" created by the short chains.

2. *Spherical grafting surface*

As mentioned earlier, the radius R of the grafting surface is five times the monomer diameter and the total chain number is $N_p = 100$. Monomer density profiles computed in this case are shown in Figs. 3(a) and 3(b). For spherical grafting surfaces, there exists a "space gradient" in the r direction, i.e., there is less space near the grafting surface and more in the outer region. The density profiles look quite different from those obtained for the flat grafting surface in the preceding subsection, but are similar to that obtained in a previous simulation of a monodisperse polymer brush grafted onto a spherical surface [15]. Throughout the inner region of the layer, the monomer density for the long chains of a brush with a particular value of short chain fraction f is almost identical to the monomer density for the short chains of the corresponding brush with a fraction $1-f$ [Fig. 3(a)]. We also observe that the total density for different values of f are very similar in the inner region, while they tend to be different only in the region far away from the grafting surface [Fig. 3(b)].

The chain-end density profiles are shown in Figs. 4(a) and 4(b). We observe that the chain ends are squeezed out of the region near the grafting surface creating a feeble "exclusion zone" [15,20–22]. Compared to the flat surface situation, the two different groups of chain ends interpenetrate each other much more in this case. Also, when the short chain fraction f changes, there is not much of a "peak shift" in the density profiles [compare Fig. 4(a) with Fig. 1(b)]. In the total end density profiles [Fig. 4(b)], we do not observe the appearance of two separated peaks as in the flat surface situation.

The above results for both the monomer density and the chain-end density suggest that for the spherical grafting case, both long and short chains stretch nearly equal amounts in the inner-most layer. This fact is clearly demonstrated in the results of $\cos\theta_i$ shown in Fig. 5. Near the surface, $\cos\theta_i$ has a large value that is nearly the same for both the long and the short chains and is independent of the short chain fraction f. It decreases fast with increasing i. Away from the narrow region near the grafting surface, we can see the difference of stretching between the long and the short chains. Long chains stretch more than short ones in this region. With the increasing of f, $\cos\theta_i$ for short chains increases throughout the layer. For long chains, $\cos\theta_i$ increases in the inner region and decreases in the outer region. However, the difference is not as large as in the flat surface case.

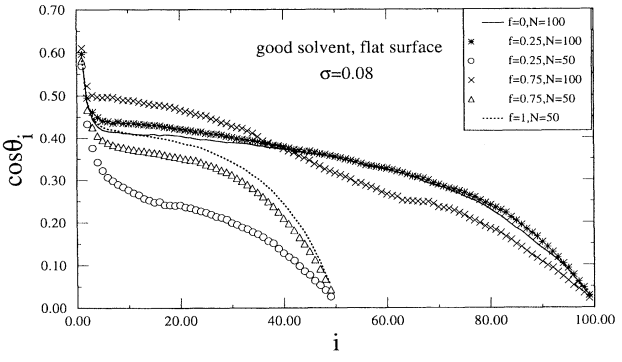

FIG. 2. Stretching parameter $\cos\theta_i$ for long and short chains of a bimodal brush grafted onto a flat surface and in contact with a good solvent for different short chain fractions f.

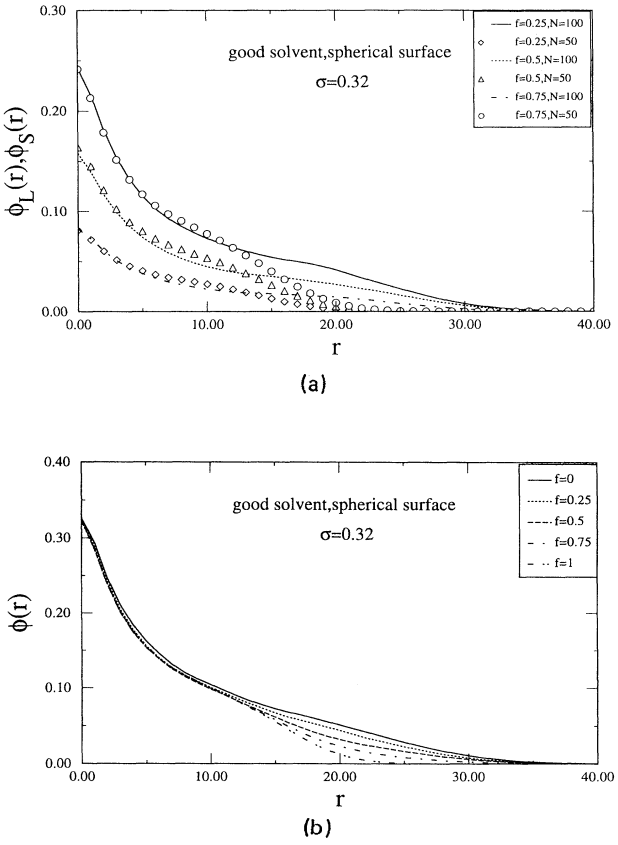

FIG. 3. (a) Density profiles for long and short chains of a bimodal brush grafted onto a spherical surface of radius $R=5$ and in contact with a good solvent for different short chain fractions f. Note that the density for the long chain of a brush with a particular value of short-chain fraction f is almost identical to the density for the short chain of the corresponding brush with a short-chain fraction $1-f$. (b) Total density profile for bimodal brush grafted onto a spherical surface of radius $R=5$ and in contact with a good solvent for different short chain fractions f.

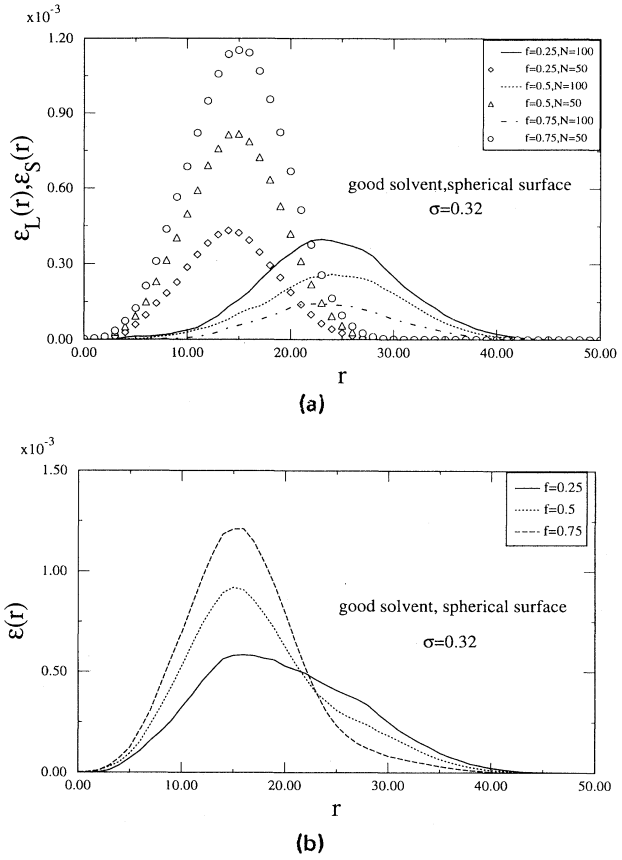

FIG. 4. (a) Chain-end density profiles for long and short chains of a bimodal brush grafted onto a spherical surface of radius $R=5$ and in contact with a good solvent for different short chain fractions f. (b) Total chain-end density profile of a bimodal brush grafted onto a spherical surface of radius $R=5$ and in contact with a good solvent for different short chain fractions f. Here we do not observe two separated peaks as in Fig. 1(b).

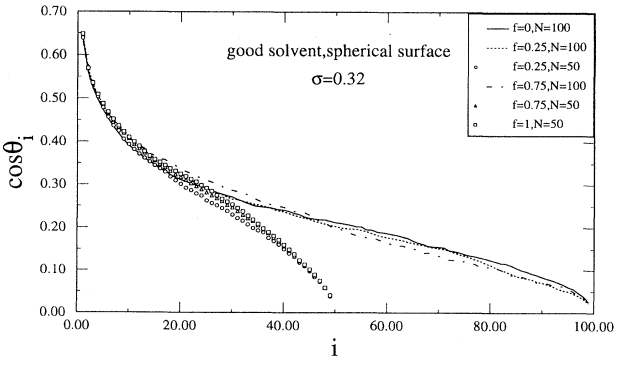

FIG. 5. $\cos\theta_i$ for long and short chains of a bimodal brush grafted onto a spherical surface of radius $R=5$ and in contact with a good solvent for different short chain fractions f. Note that $\cos\theta_i$ is nearly independent of chain type and short chain fraction f near the grafting surface.

B. Chains in poor solvents

Here the interaction potential between monomers is described by Eq. (1). We choose several different values of V_0 corresponding to different solvent qualities. Note that $V_0=0$ corresponds to good solvents, while for $V_0=V_C\approx 0.1335$ the excluded volume parameter $\omega\approx 0$ [Eq. (2)]. This latter choice of V_0 would then approximately correspond to a Θ solvent. We have also considered $V_0=1.5V_C$ and $2.5V_C$, which would correspond to two different poor solvents.

1. Flat grafting surface

Results for the grafting density $\sigma=0.08$ and a fixed short chain fraction $f=0.5$ are shown in Figs. 6 and 7. Monomer densities for the long and short chains are shown in Fig. 6(a). As the solvent quality becomes worse, the attractive interaction between monomers increases. However, due to the presence of a hard-sphere repulsion, the chains do not collapse completely and the peaks for the long and the short chains are separated out. As V_0 increases, these two peaks move closer to each other. With decreasing solvent quality, the total density profile [Fig. 6(b)] shrinks to a narrower region near the surface and gets higher and flatter while it gets sharper at the edge. For the values of V_0 considered here, we did not observe any "crystallization" of monomers as seen by Lai and Binder [23] in their bond fluctuation model of a monodisperse brush in a poor solvent. Snapshots of chain configurations indicate that the monomers are confined to a very narrow region near the grafting surface for poor solvents. However, they are distributed uniformly and in the chain configurations we do not find any obvious signature of a microphase separation [23–26] for the values of σ, N, and V_0 considered here.

There are several interesting features in the monomer density profiles for poor solvents. First, we observe that the long chain density has a "shoulder" near the peak of the short chain profile. This is due to the strong attractive interaction between the monomers. Another interesting feature of the profiles is that the short chain density profile spreads into almost all the region where the long one exists, implying very little vertical segregation between the long and short chains. This is also evident in the chain-end density shown in Fig. 6(c). In poor solvents, the chain-end densities for the long and short chains extend the same distance from the grafting surface.

In Fig. 7 we present the results for $\cos\theta_i$ for both long and short chains. As the solvent quality worsens, $\cos\theta_i$ decreases for both long and short chains. The stretching of the long chains and of the short chains is similar. Actually, for $V_0=1.5V_c$, one can say that the short chains are actually a little more stretched than the long chains in the coexisting region of the layer. This is in strong contrast to the situation in a good solvent. For larger V_0, however, $\cos\theta_i$ shows large fluctuations, implying that the orientation of the segments is not strongly correlated in the z direction and none of the chains are really stretched [23].

We also examined the influence of short chain fraction f on the behavior of bimodal chains in poor solvent. We choose $V_0=1.5V_C$ and $f=0,0.25,0.75,1$. Our results for $\cos\theta_i$ are shown in Fig. 8. In poor solvent situation, we find that as f increases, the short chains become less stretched. This is in sharp contrast to the situation in a good solvent, where the stretching parameter for the short chains increases as the short chain fraction f increases (compare Fig. 8 with Fig. 2). For the long chains the stretching parameter also decreases over the entire region as the short chain fraction increases.

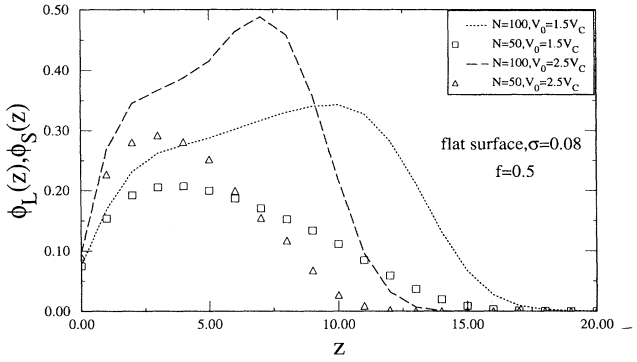

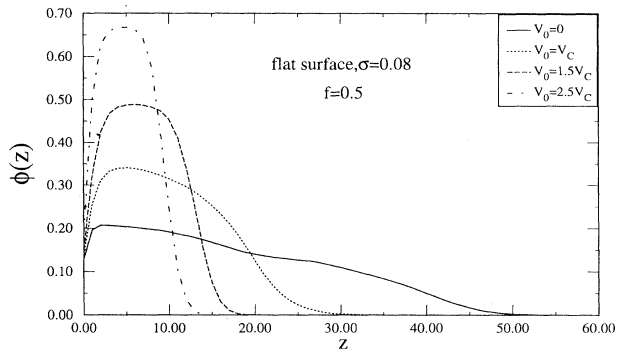

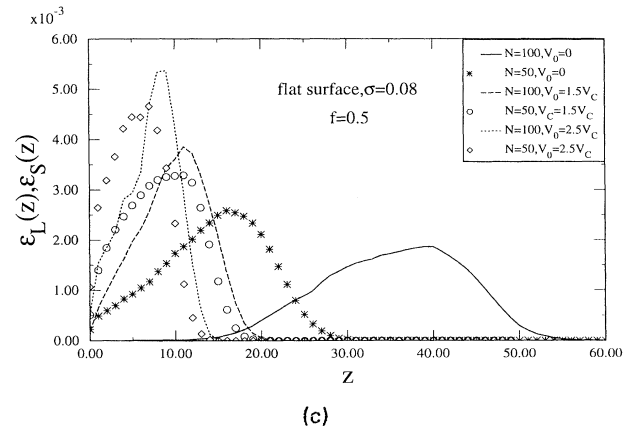

FIG. 6. (a) Density profiles for long and short chains of bimodal brushes grafted onto a flat surface for different solvent conditions. The short chain fraction $f=0.5$. (b) Total density profile for bimodal brushes grafted onto a flat surface for different solvent conditions. The short chain fraction $f=0.5$. (c) Chain-end density profiles for long and short chains of bimodal brushes grafted onto a flat surface for different solvent conditions. The short chain fraction $f=0.5$.

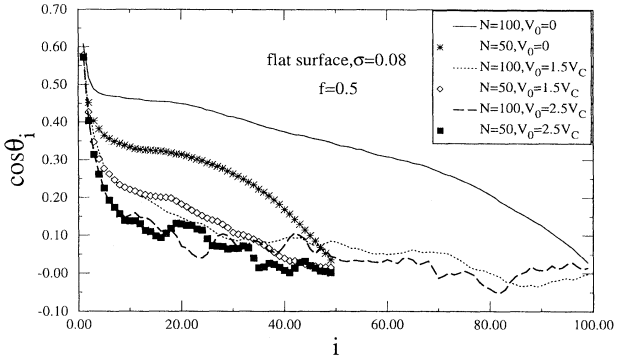

FIG. 7. Stretching parameter $\cos\theta_i$ for long and short chains of bimodal brushes grafted onto a flat surface for different solvent conditions. The short chain fraction $f=0.5$.

2. *Spherical grafting surface*

In this case, the general behavior of the long and short chains with the changing of solvent quality is quite similar to that for a flat grafting surface. In Fig. 9 we show the density profiles for $f=0.5$. In contrast to the good solvent case, where the density profile for the short and long chains is identical in the innermost layer, the shape of the density profiles for the long and short chains is different in poor solvents [Fig. 9(a)]. The density profiles now develop peaks not seen in good solvent condition. These peaks for the long chains and the short chains are close but still separated. However, the extension of the sublayers is the same for both long and short chains. The total density profiles in poor solvent condition look similar to those obtained with a flat grafting surface [Fig. 9(b)]. The stretching of the chains decreases as the sol-

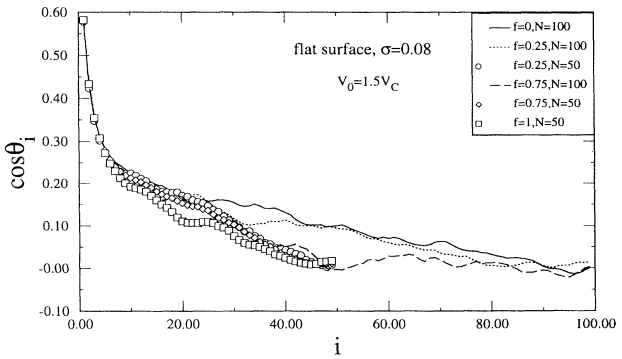

FIG. 8. Stretching parameter $\cos\theta_i$ for long and short chains of bimodal brushes grafted onto a flat surface for different short chain fractions f. Here the solvent is a poor solvent and characterized by $V_0=1.5V_C$ (see the text).

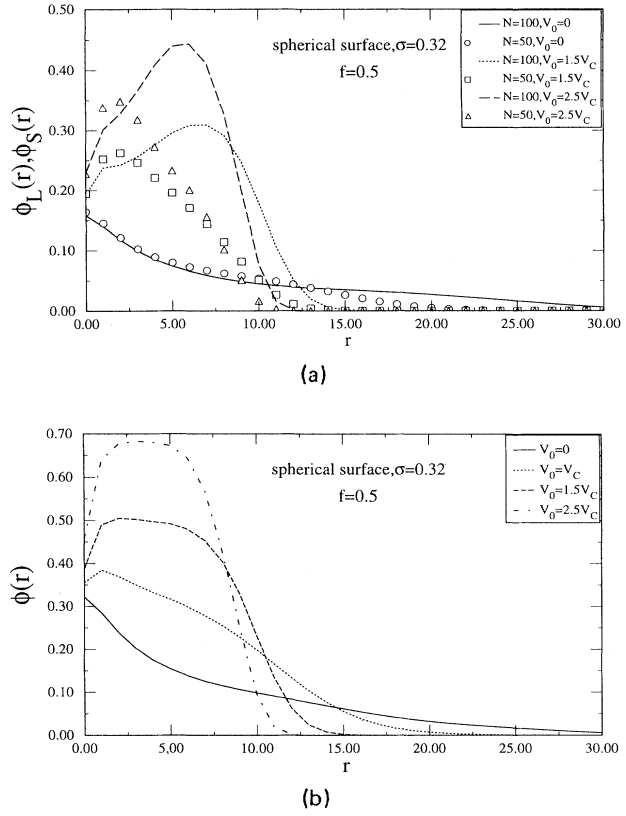

FIG. 9. (a) Density profile for long and short chains of bimodal brushes grafted onto a spherical surface of radius $R=5$ for different solvent conditions. The short chain fraction $f=0.5$. (b) Total density profile of bimodal brushes grafted onto a spherical surface of radius $R=5$ for different solvent conditions. The short chain fraction $f=0.5$.

vent quality becomes poorer and for $V_0=1.5V_c$ both the long and short chains stretch almost the same amount throughout the layer.

IV. CONCLUDING REMARKS

We have carried out off-lattice computer simulations to study the structure of bimodal brushes grafted onto both flat and spherical surfaces and in contact with either good or poor solvents. The results for flat grafting surface and good solvents compare well with previous analytical results and simulations carried out in different models for polymer chains. In this case, we find that the short and long chains segregate vertically and the long chains stretch more in the coexisting region. The situation is different with polymers grafted onto flat surface and in contact with poor solvents. We find that the long and short chains do not segregate vertically by an appreciable amount and the amount of stretching for each type of chains is quite similar. Actually, in some poor solvent condition, the short chains are found to stretch a little more than the long chains. Also, as the fraction of short chains increase in the layer, both the short and the long chains stretch less. This is different from the good solvent case, where the stretching parameter for the short chains increases as f increases.

For a spherical grafting surface and in good solvents, the short and long chains are not as segregated as in a flat grafting surface. The stretching of the two types of chains is similar in the inner layer and is dictated by the availability of space near the spherical grafting surface. In poor solvent conditions, the situation is similar to the flat grafting case and both type of chains are equally stretched over the entire region of the layer.

The simulation results agree well with self-consistent field theories for flat grafting surfaces and good solvents. For poor solvents and for spherical grafting surfaces, we could not compare our results with theories, since no theoretical result for bimodal brushes are available in the literature for such conditions. We note that recent mean-field calculations for the structure of the monodisperse brush in good solvents and grafted on a spherical surface [27] compare quite well with our previous numerical results [15] in such systems. Similar theoretical work also exists for mixed micelles and bilayers [28]. More importantly, recent surface force experiments [14] have measured the interactions between two mixed brushes in a selective solvent. We hope that our numerical results will motivate further theoretical work and a quantitative comparison between theory, simulation, and experiments will be possible in the near future.

ACKNOWLEDGMENTS

We thank Dr. J. Marko for many useful comments and Professor H. Guo, Professor I. Szleifer, and Professor M. Tirrell for sharing results with us prior to publication. This material is based upon work supported by the National Science Foundation under Grant No. OSR-9255223 (NSF-EPSCoR).

[1] See, for example, W. B. Russel, D. A. Saville, and W. R. Schowalter, *Colloidal Dispersions* (Cambridge University Press, Cambridge, 1989).
[2] H. J. Taunton, C. Toprakcioglu, L. J. Fetters, and J. Klein, Nature **332**, 712 (1988).
[3] P. Auroy, L. Auvray, and L. Leger, Phys. Rev. Lett. **66**, 719 (1991).
[4] P. Auroy, Y. Mir, and L. Leger, Phys. Rev. Lett. **69**, 93 (1992).
[5] P. Auroy and L. Auvray, Macromolecules **25**, 4134 (1992).
[6] A recent review is given by S. T. Milner, Science **251**, 905 (1991).
[7] For a review, see also A. Halperin, M. Tirrell, and T. P. Lodge, Adv. Polym. Sci. **100**, 31 (1991).
[8] A recent review is given by G. S. Grest and M. Murat (unpublished).
[9] S. T. Milner, T. A. Witten, and M. E. Cates, Macromolecules **22**, 853 (1989).

[10] T. M. Birshtein, Y. V. Liatskaya, and E. B. Zhulina, Polymer **31**, 2185 (1990).
[11] A. Chakrabarti and R. Toral, Macromolecules **23**, 2016 (1990).
[12] P. Y. Lai and E. B. Zhulina, Macromolecules **25**, 5201 (1992).
[13] N. Dan and M. Tirrell, Macromolecules **26**, 6467 (1993).
[14] C. Chen. N. Dan, S. Dhoot, M. Tirrell, J. Mays, and H. Watanabe (unpublished).
[15] R. Toral and A. Chakrabarti, Phys. Rev. E **47**, 4240 (1992).
[16] R. Toral, A. Chakrabarti, and R. Dickman, Phys. Rev. E **50**, 343 (1994).
[17] S. F. Edwards, Proc. Phys. Soc. London **85**, 613 (1965).
[18] Note that the numerical value of the excluded-volume parameter computed in previous simulations of polymer brushes in good solvents [16] differs from that obtained from the above expressions for ω.
[19] S. T. Milner, T. A. Witten, and M. E. Cates, Macromolecules **21**, 2610 (1988).
[20] R. C. Ball, J. F. Marko, S. T. Milner, and T. A. Witten, Macromolecules **24**, 693 (1991); H. Li and T. A. Witten, *ibid.* **27**, 449 (1994).
[21] M. Murat and G. S. Grest, Macromolecules **24**, 704 (1991).
[22] N. Dan and M. Tirrell, Macromolecules **25**, 2890 (1992).
[23] P. Y. Lai and K. Binder, J. Chem. Phys. **97**, 586 (1992).
[24] G. Grest and M. Murat, Macromolecules **26**, 3108 (1993).
[25] C. Yeung, A. C. Balazs, and D. Jasnow, Macromolecules **26**, 1914 (1993).
[26] K. G. Soga, H. Guo, and M. J. Zuckermann (unpublished).
[27] M. A. Carignano and I. Szleifer (unpublished).
[28] I. Szleifer, A. Ben-Shaul, and W. M. Gelbart, J. Chem. Phys. **86**, 7094 (1987).